esteem3

Enabling Science through European Electron Microscopy

First report on TEM methods applied to materials for transport
Deliverable D10.1 – version 0.5

Estimated delivery date: M16 April 2020

Actual delivery date: M16 April 2020

Lead beneficiary: KRA, TRO

Person responsible: Adam Kruk, Randi Holmestad

Deliverable type: ☒ R ☐ DEM ☐ DEC ☐ OTHER ☐ ETHICS ☐ ORDP

Dissemination level: ☒ PU ☐ CO ☐ EU-RES ☐ EU-CON ☐ EU-SEC

Grant Agreement No:	823717
Funding Instrument:	Research and Innovation Actions (RIA)
Funded under:	H2020-INFRAIA-2018-1: Integrating Activities for Advanced Communities
Starting date:	01.01.2019
Duration:	48 months

Table of contents

Revision history log

Version number	Date of release	Author	Summary of changes
V0.1	10.03.2020	Adam Kruk	Preparation of the initial version of the report.
V0.2	23.03.2020	Trondheim node (Randi Holmestad Dipanwita Chatterjee, Tina Bergh, et al)	Gone through report, added parts
V0.3	26.03.2020	Adam Kruk Grzegorz Cempura	Final editing correction
V0.4	06.04.2020	Lucie Guilloteau	Amendment of the draft
V0.5	07.04.2020	Peter van Aken	Approval of the deliverable

Task 10.1: Sample preparation for materials for transport (KRA, TRO, TOU, LJU)

The aim of this task is the implementation of sample preparation methods for various "difficult" materials such as Ni-based superalloys, advanced high-strength steels (AHSS), Ti, Al and Mg-based alloys and fibre reinforced composite materials using different techniques for preparing thin artefact free TEM lamellae. High-quality electron transparent thin specimens are essential for state-of-art TEM/STEM investigations. Excellent samples are necessary for an examination of a structural element at an atomic scale. This is why a great effort has been put into optimization of the existing sample preparation techniques, such as tripod polishing, ion milling, FIB techniques, electro-polishing and ultramicrotomy. New techniques for preparing sensitive samples were also investigated. Finally, protocols for sample preparation were prepared and published on-line on the ESTEEM3 website.

Preparing a FIB lamella for TEM is usually started with the deposition of a protective layer. Such a thin layer is mandatory to protect the sample from any damages that could occur with thick layer (several µm) made by ion-induced deposition (IBID). This layer is used for protection of the sample from any damage in the whole FIB preparation procedure. When preparing a sample for transmission microscopy, we want the lamellas to contain elements of microstructure that are of interest to us from the analysis point of view. ***To make this happen, we suggest combining FIB-SEM tomographic acquisition of images with lamella cutting, Targeted Sample Preparation (TSP).***
FIB-SEM tomography combined with targeted TEM specimen preparation was adopted for TEM investigation of welded alloys: Inconel 718/Allvac 718Plus weld joint. Sample preparation in the form of lamellae from the chosen area of the weld material - targeted cutting, what was presented on Fig.10.1.1.
A protocol for Targeted Sample Preparation (TSP) for TEM will be prepared.
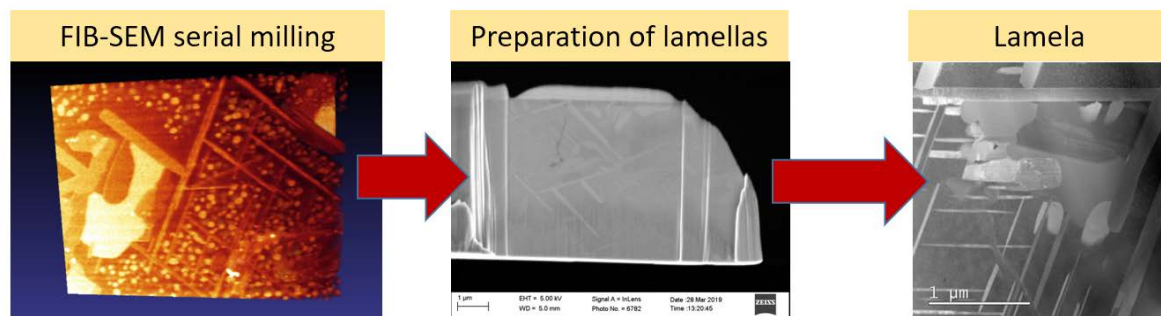
Fig.10.1.1. The combination of FIB-SEM tomography with targeted sample removal from the analysed volume of sample for TEM studies -Targeted Sample Preparation (TSP).

Sample preparation for TEM tomography from Allvac 718Plus nickel-based superalloy.

Tomographic investigations of Ni-based superalloys will provide additional informations about the microstructural features. Therefore, within the task we decided to prepare some specimens according to the method developed in Graz. The samples were prepared in cooperation with TU Graz. Information about the preparation and the finished tips (Fig.10.1.2.):

· Specimen was cut in 3 pieces to prepare 3 nanotips.

·   Cross-section of the specimens from Kraków wasn't square-shaped, more parallelogram-shaped.

·   One specimen has been ground to a square cross-section. Due to the small cross-section, the grinding was difficult and the risk of destruction high. Therefore, only one specimen (tip 1) has been ground.

·   Quality of the ground sample is much higher than of the others.

·   Used Electrolyte: 2 vol% perchloric acid (60 wt %) in 2-butoxyethanol.
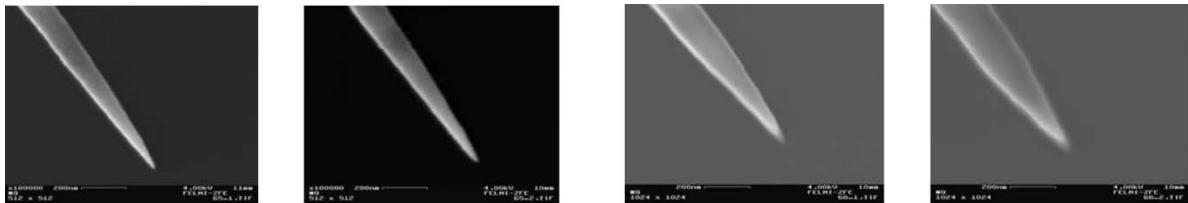
Fig.10.1.2. Sample prepared for TEM tomography from Allvac 718Plus nickel-based superalloy.

Sample preparation for in-situ heating in TEM.

Lamellae of age-hardening aluminium alloys on DENS chips for in-situ heating in TEM were prepared using electropolishing plus FIB techniques to get the best quality samples in the correct orientations (**Fig.10.1.3.**). The procedure is as following:

1) Electropolishing (standard preparation using a Struers Tenupol with an electrolyte consisting of 1/3 HNO_3 and 2/3 Methanol).
2) Study the electropolished disk in TEM to locate thin grains close to [001] zone axis.
3) FIB lift-out:
   - Mill out [001] grain,
   - attach the lift-out needle to the thicker part of the grain with C welding,
   - attach the lamella to the DENS chip using C welding, and
   - cut off the lift-out needle.
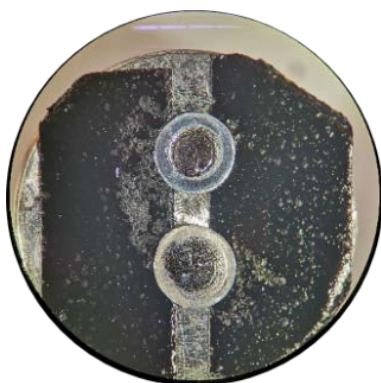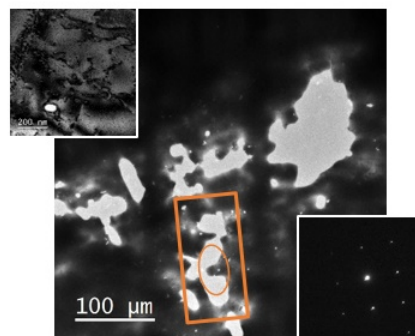
1) Electropolishing   2) TEM: find [001] grains
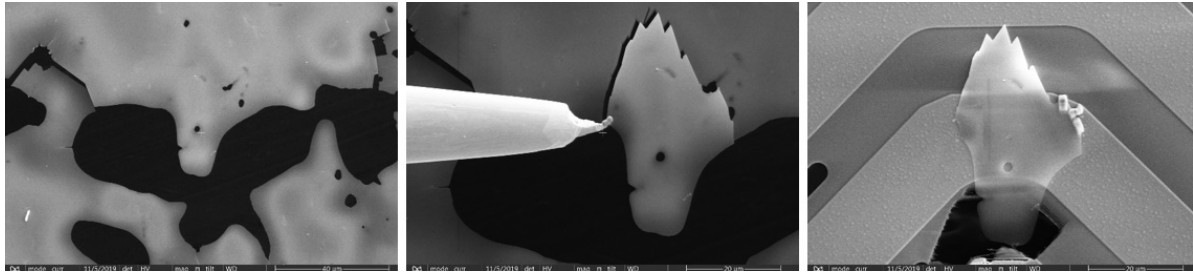
3) FIB lift-out of a [001] oriented aluminium grain

Fig.10.1.3. Overview of the aluminium lamellae preparation for in-situ heating in TEM. Results from NTNU TRO.

The quality gets best by never exposing the region of interest (ROI) to the ion beam. It is crucial to limit redeposition on the ROI by performing all milling and welding more than ~20 μm from the ROI. In this way it is possible to achieve close to electropolished surface quality by combining electropolishing and FIB lift-out to get a site-specific area in the correct zone axis (Fig.10.1.4.). This gives superior quality compared to previous work [1].
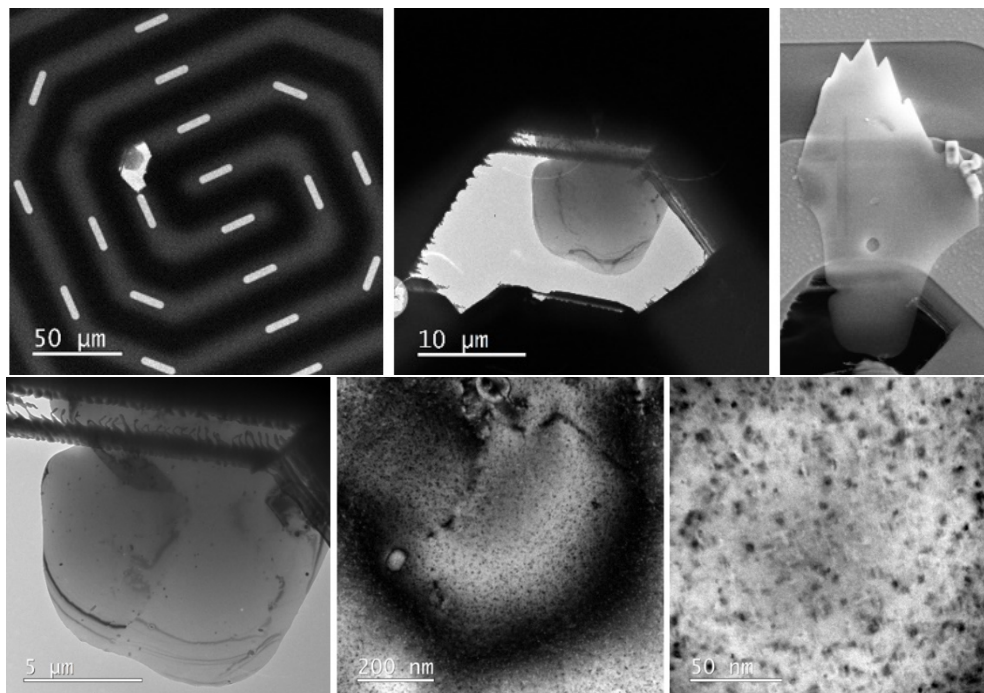
Fig.10.1.4. BF-TEM images and a SEM image (top right) of an aluminium lamella attached to a DENS chip for in-situ heating in TEM. Results from NTNU TRO.

Task 10.2: Materials for Aeronautics/Aerospace (KRA, TRO, TOU)

This task presents the results of the application of analytical TEM and FIB-SEM tomography techniques to perform detailed characterisation (visualization and phases identification) of structural elements in various engineering materials. The KRA team investigates the structure of inorganic materials in the view of their application for aeronautics, among them Ni-base superalloy Inconel 718Plus Allvac; those results are presented below. Specific challenges include the identification and detailed characterization at the nanoscale of various advanced structural and functional materials, implementing various diffraction, spectroscopy and data analysis techniques. Application of high-resolution SEM and TEM to a detailed characterization of structural elements in EBW dissimilar Inconel 718/ALLVAC® 718PLUS welded joint. The effects of welding and post welding heat treatment on the microstructure of the fusion zone of Inconel 718/Allvac718Plus welded joint was analysed. **Figure 10.2.1** present SEM microphotographs of the fusion zone microstructures and shows the phase transformation in the fusion during exposure at 640 °C and 760 °C.
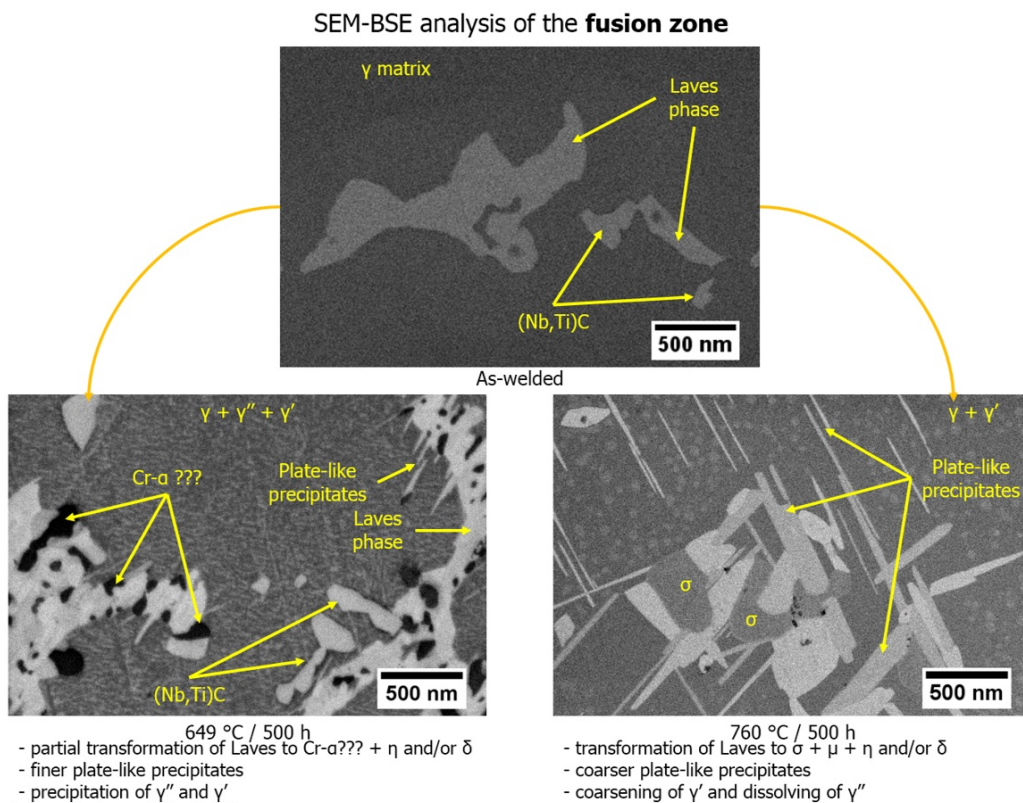
Fig.10.2.1. The phase transformation in the fusion during exposure at 640 °C and 760 °C, SEM-BSE.

Inconel 718 and ATI 718Plus belong to a group of the precipitation-hardened Ni-base superalloys. The above-mentioned alloys feature high strength and excellent corrosion resistance combined with relatively good weldability. Fusion welding leads to microsegregation during weld metal solidification. This phenomenon may result in the formation of low melting temperature eutectics and/or brittle phases in the interdendritic regions of the fusion zone. These microstructural constituents have an important effect on the mechanical properties of the welded joint. Allvac 718Plus (718Plus) is a high

strength, corrosion-resistant nickel-based superalloy, designed to replace Inconel 718 superalloy (IN718) in some application in power generation and aerospace industry. In comparison to IN718, the 718Plus shows improved temperature performance. Its chemical composition is: Ni-18-Cr-10-Fe-9Co-5.1(Nb+Ta)-1W-2.7Mo-0.8Ti-1.5Al-00.3C (wt %). The post welded heat treatment leads to the precipitation of γ'-Ni_3(Al,Ti) in all alloy volume and platelet precipitates of η-Ni_3Ti phases nucleating at Laves phase (Fig.1). The microstructure of the fusion zone consists of a γ dendrite matrix with two kinds of eutectics: (MC–type carbides + γphase) and (Laves-phase + γ-phase) precipitates in the inter-dendritic region.

The aim of presented results was the analysis of the Laves phase transformation in the fusion zone of the electron beam welded dissimilar Inconel 718/ATI 718Plus joint during exposure at 760 °C. FIB-SEM tomography was employed to reveal the shape and spatial distribution of selected microstructural features within the weld metal. Visualization in 3D of the tomographic reconstructed volume of material from the fusion zone region after exposure at 760 °C for 500h was presented on Fig.10.2.2. For 3D visualization of precipitates, a FIB-SEM technique was employed utilizing NEON CrossBeam 40EsB (ZEISS, Germany) microscope with Ga-ion beam. In-lens, secondary- and Energy-selective Backscattered (EsB) electron images were obtained using a beam with parameters of 1.5 kV and 50 pA. In-situ milling was conducted using an ion beam operating at 30 kV, 50 pA with 30 μm aperture. Tomographic reconstruction was prepared as follows: at first, the region of interest (ROI) was identified by SEM imaging and coated by a protective platinum layer to prevent any negative preparation effects, such as curtaining effect, and make the further process more stable.

Voxel size: 8 x 8 x 8 nm   V = 7.25 x 3.62 x 6.32 μm
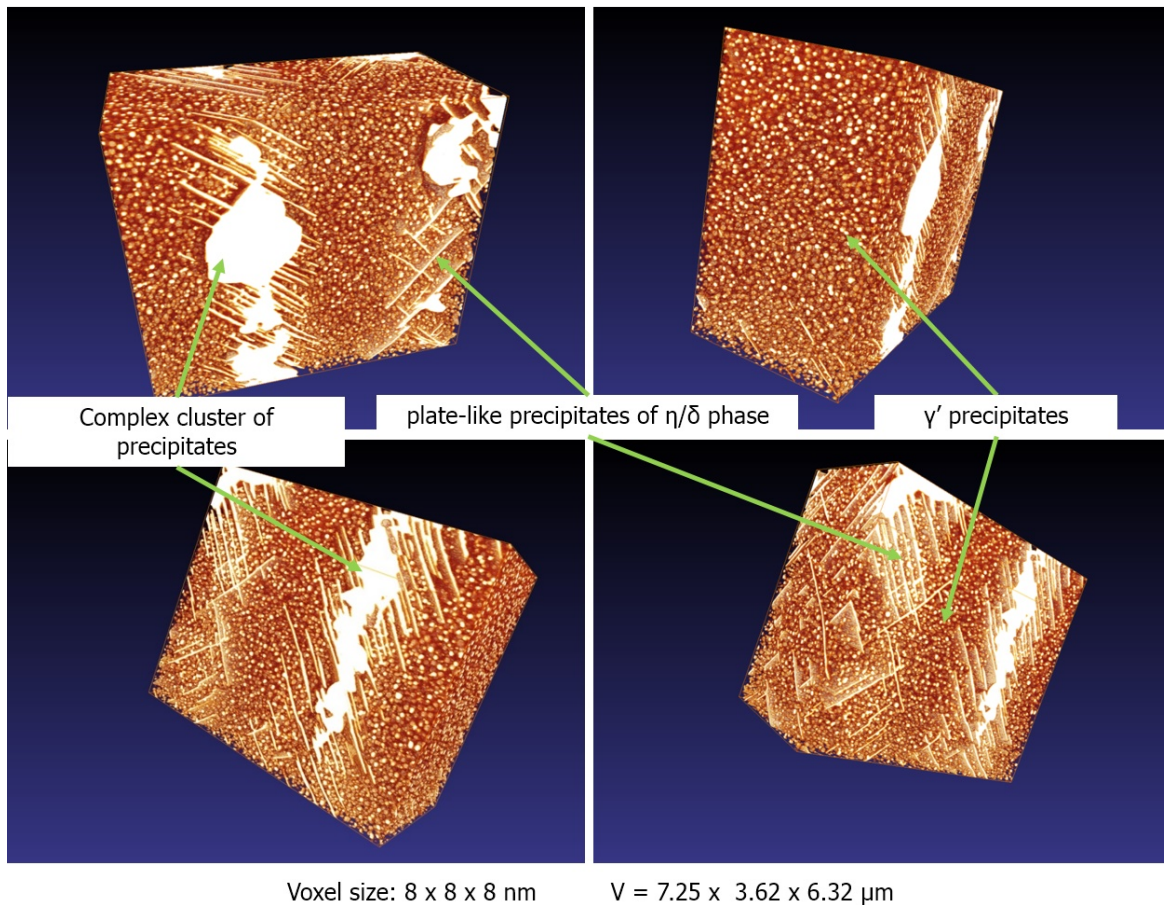
Fig.10.2.2. Visualization in 3D for different view directions of the tomographic reconstructed volume of material from the fusion zone region after exposure at 760 °C for 500h.

Stack of 146 SEM images (image size 1024 x 768 pixels, 8-bit grayscale, stack size 113 MB) was acquired from the cross-section of the investigated sample. Sequential removal of 8 nm layers allowed to acquire 7.25 x 3.62 x 6.32 µm (V = 165.9 µm³) total volume for further analysis and reconstruction with a voxel size of 8 × 8 × 8 nm. All the data processing, including image shift corrections, image analysis and 3D visualizations were performed using open source Fiji software. The same image analysis was applied for each image in the reconstructed stack even though contrast in some slices was slightly different. This approach allowed minimizing the subjective analysis factor. The nearest-neighbourhood algorithm was used for object segmentation, thus nearby voxels with the same and similar grey levels were assigned to one object. 3D visualization of the reconstructed volume was done using Avizo Fire 6.3 software (ThermoFisher, USA). The investigations were performed using scanning electron microscopy (SEM) and high-resolution scanning transmission electron microscopy (HRSTEM) supported by energy-dispersive X-ray spectroscopy (XEDS). To identify phases present in the weld metal before and after isothermal hold, selected area electron diffraction (SAED) supported by Java Electron Microscopy Software (JEMS 4.81) was used. The fusion zone in the as-welded condition has an as-cast structure with dendrites of the γ matrix surrounded by interdendritic regions consisted of MC-type carbides and Laves phase precipitates within the γ matrix. Exposure of the welded joint at 760 °C prompted a string of microstructural changes in the fusion zone. Reprecipitation and growth of main strengthening phases' particles occurred. Figure 10.2.3 present results of the chemical composition of individual phases (δ, η, σ, γ) investigations of post welded heat treatment (PWHT) the fusion zone (760 °C / 500 h) using STEM-XEDS technique [2].
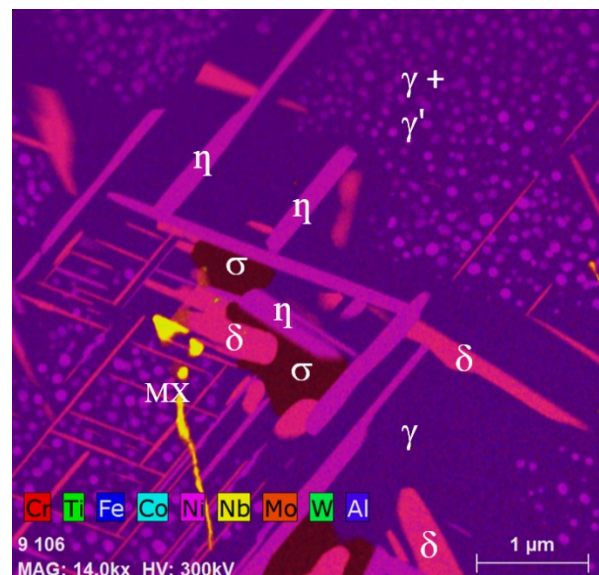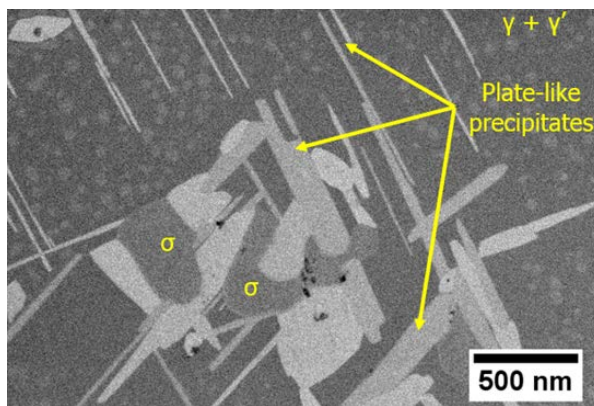
	Cr-KA	Ti-KA	Fe-KA	Co-KA	Ni-KA	Nb-KA	Mo-KA	W-LA	Al-K	
δ	1.35	1.57	1.82	3.99	67.13	19.15	2.27	0.32	2.40	Ni, Nb, Ti
	0.63	0.18	0.44	0.26	1.07	0.62	0.35	0.10	0.53	
η	0.77	4.05	1.84	3.57	65.82	11.46	0.75	0.27	11.49	Ni, Nb, Al., Ti
	0.07	0.26	0.19	0.11	0.59	0.91	0.17	0.08	0.56	
σ	46.14	0.15	12.86	7.61	18.47	0.54	10.93	0.98	2.33	Cr, Mo, Co
	0.50	0.05	0.16	0.21	0.34	0.11	0.21	0.08	0.26	
γ	23.65	0.25	16.80	6.93	47.00	0.90	1.80	0.30	2.38	Cr, Fe, Co, Ni
	0.20	0.03	0.07	0.09	0.27	0.05	0.09	0.02	0.04	

Fig.10.2.3. SEM, STEM-XEDS investigations of PWHT the fusion zone (760 °C / 500 h). Averaged chemical composition of individual phases (δ, η, σ, γ) in at.%.

Round robin test (AGH-TRO) for determination of the chemical composition of different phases present in investigated area of weld metal was performed in NTNU TRO. Example results of the application of STEM – EDX for detailed characterization of the chemical composition of structural elements in fusion zone EBW Inconel 718/ALLVAC® 718PLUS welded joint was presented in Fig.10.2.4. To fully investigate the microstructural features of 718Plus detailed characterization was performed using precession electron diffraction techniques-PED. Round robin test (AGH-TRO) for phase analysis performed on this same lamella present in the investigated area of weld metal was presented as selected results from TEM-SPED analysis in Fig.10.2.5.
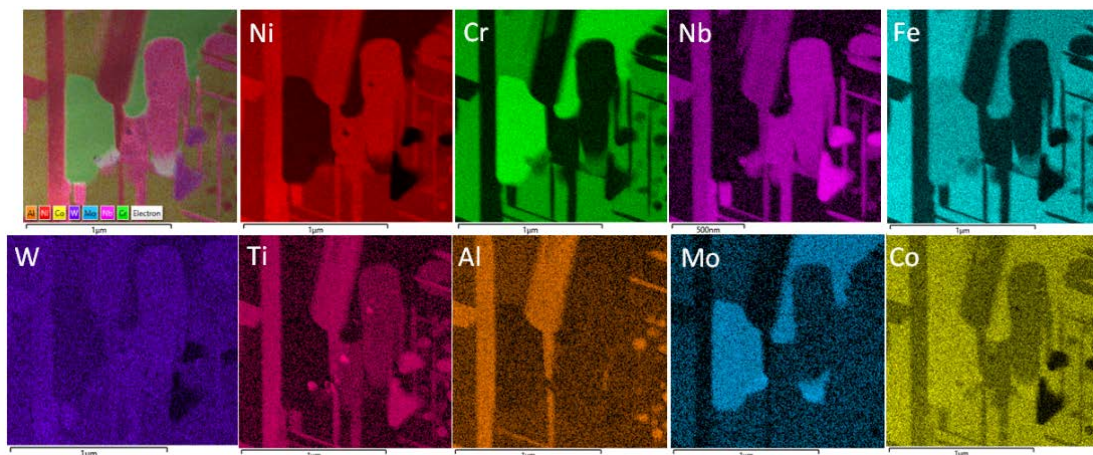
Fig.10.2.4. STEM-XEDS investigations of PWHT the fusion zone (760 °C/500 h). EDS maps from the fusion zone showing different elements (qualitative maps, TRO).
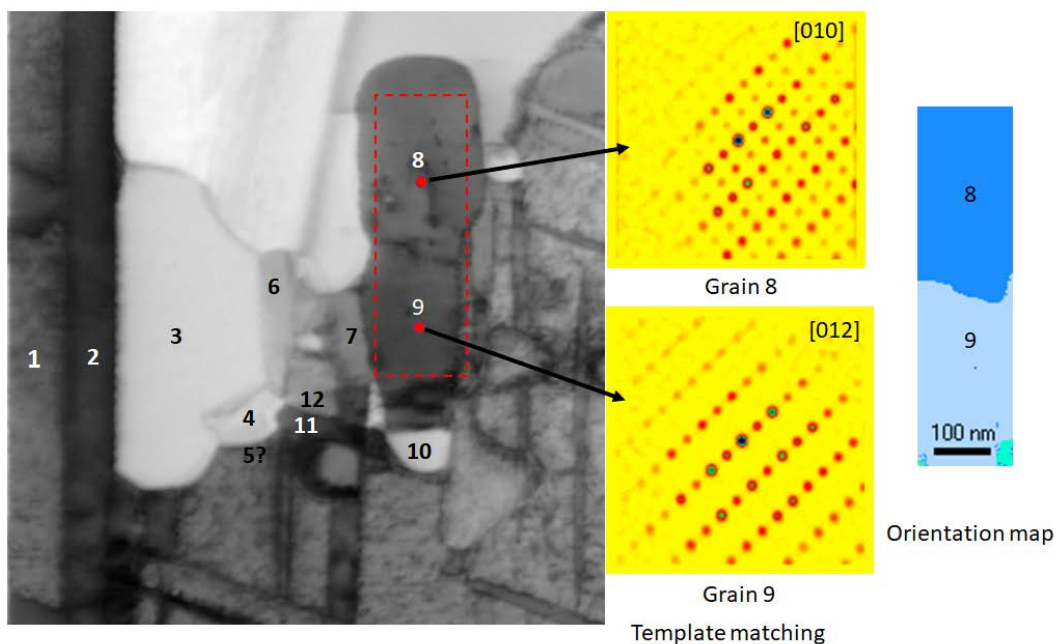
Fig.10.2.5. Round robin test (AGH-TRO) for phase analysis present in the investigated area of weld metal. Selected SPED results from the grains in the fusion area. Orientation map was obtained after template matching.

Furthermore, a transformation of the Laves phase to a complex cluster of precipitates enclosed both μ and σ phases had taken place. Precipitates enriched in Mo and W were identified as trigonal μ phase, whereas other areas enriched in Mo, W and Cr – as tetragonal σ phase. Moreover, plate-like precipitates of δ/η phases growing from the complex cluster of precipitates' surfaces were observed (Fig. 10.2.6).
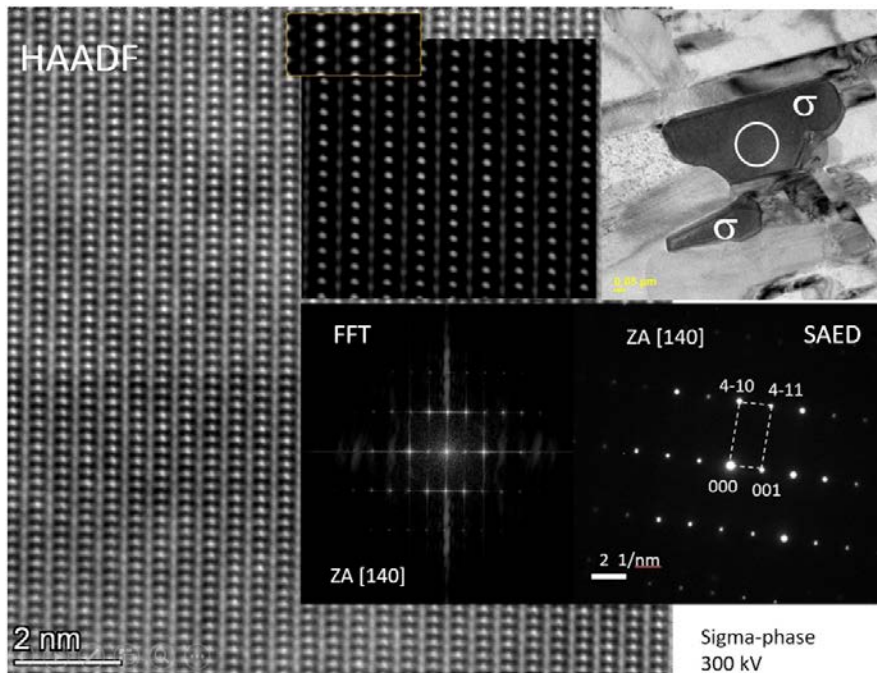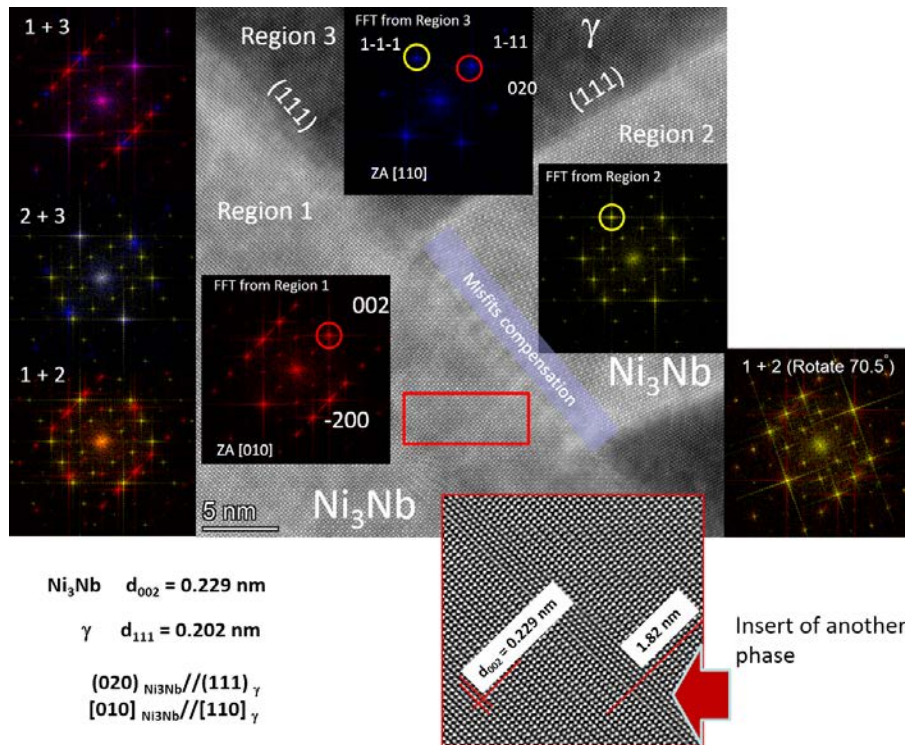
Fig.10.2.6. The high-resolution TEM analysis of sigma and delta phases which is a result in Laves phase transformation during post-heat treatment of welded joints.

Round-Robin tests conducted by the partners (KRK, TRO) provided important information on the reproducibility of the results that were obtained using the same procedures by different laboratories using different microscopes.

Task 10.3: Materials for Automotive Body and Chassis Structure (TRO, KRA, TOU)

This task will focus on materials for automotive body and chassis structures including AHSS, as well as Ti, Al and Mg based alloys and advanced composites. AHSS are complex materials, with carefully selected chemical compositions and multiphase microstructures resulting from precisely controlled thermal processing. Within this group of materials various strengthening mechanisms are also employed to achieve a wide range of strength, ductility, toughness, and fatigue properties. Advanced composite materials include fibre-reinforced materials that offer a wide range of advantages to the automotive industry, e.g. the potential for saving weight. Aluminium alloys give an optimal combination of strength, corrosion susceptibility and ductility and are optimised by tailoring the properties of each component. Combinations of innovative heat treatments and compositions result in a complex combination of strengthening precipitates in the Al matrix, whose effects on the properties are not well understood.

We will identify phases and characterise various advanced structural materials for body and chassis structures, for example the ultralight steel auto body (ULSAB) which has demonstrated a 19% mass reduction in a body structure with superior strength and structural performance.

Our specific objectives will be:

- Phase identification and detailed characterisation of innovative structural and functional materials.

- Characterisation of joined micro- and nanostructures in materials for automotive body and chassis structures.

- Implementation of in situ straining and heating (WP6) combined with automated orientation mapping.

Studies of grain boundaries in 7xxx Al alloys. This is a Round robin test (AGH-TRO) to study precipitates at grain boundaries in an extruded AA7003 alloy which is susceptible to stress corrosion cracking (SCC) [3]. Phase, size, shape and density of grain boundary precipitates and/or grain boundary density determine the SCC. The objective is to get a more statistical study of the different types of grain boundaries, preferably in 3D, over number of precipitates, misorientation and crystallographic nature of the grain boundaries. Fig. 10.3.1 shows a SCC attack, and images of grain boundaries in this material. Angle dependent precipitates process at grain boundaries were observed (Fig.10.3.2) using SEM analysis. The high density of small precipitates at low angle grain boundaries (LAGB) was also observed.
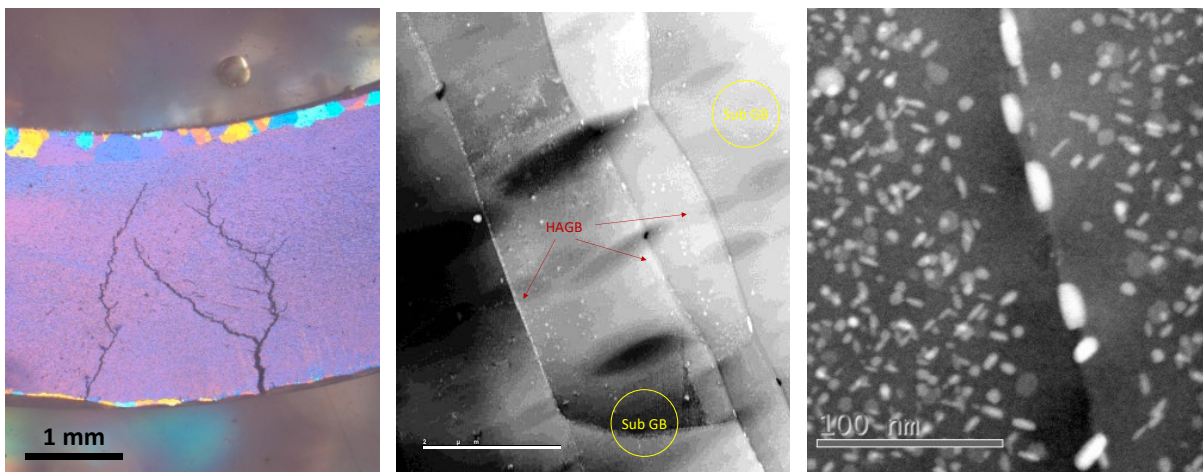
Fig. 10.3.1. SCC attack and grain boundaries in a 7003 Aluminium alloy.
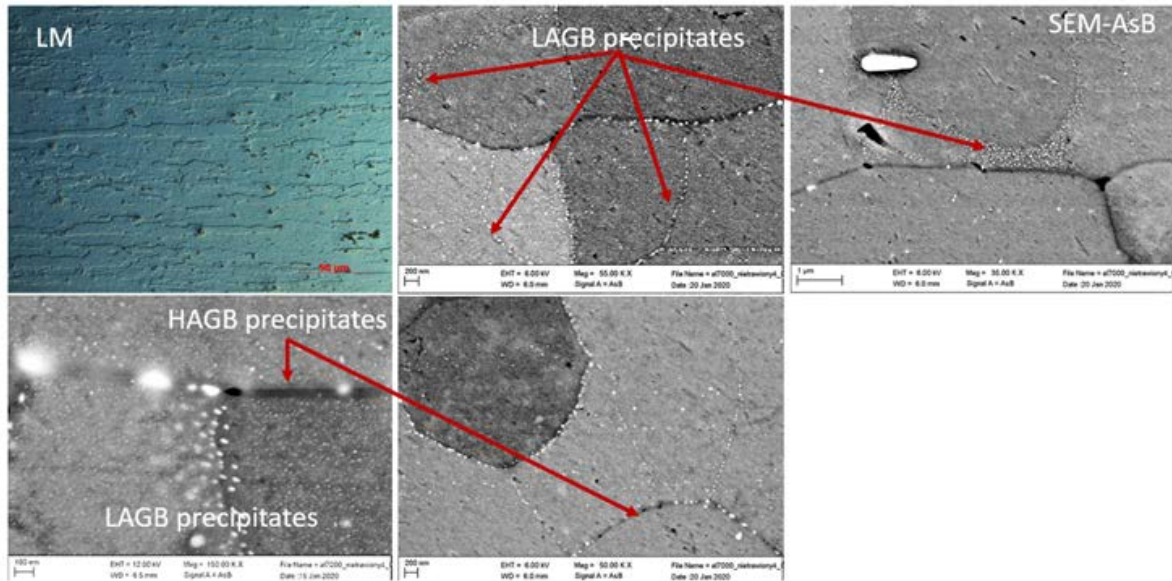
Fig.10.3.2. Preliminary results of the analysis of the precipitates precipitated at grain boundaries in an extruded AA7003 alloy, SEM analysis.

Publications

[1] JK Sunde, S Wenner and R Holmestad, In situ heating TEM observations of evolving nanoscale Al–Mg–Si–Cu precipitates, Journal of Microscopy, online (2019), https://doi.org/10.1111/jmi.12845

[2] O. Dziuba, G. Cempura, A. Wusatowska-Sarnek, A. Kruk, *Influence of Isothermal Holding on the Microstructure and Mechanical Properties of EBW Dissimilar Inconel 718/ATI 718Plus® Welded Joint*, Journal of Materials Engineering and Performance (will be published in 2020). DOI: 10.1007/s11665-020-04583-6

[3] A Lervik, CD Marioara, M Kadanikd, JC Walmsley, B Milkereit and R Holmestad, Precipitation in an extruded AA7003 aluminium alloy: Observations of 6xxx-type hardening phases, Materials & Design, 186 (2020) 108204, 10.1016/j.matdes.2019.108204